All-Angle Negative Refraction for Surface Plasmon Waves Using a Metal-Dielectric-Metal Structure

Hocheol Shin and Shanhui Fan

Department of Electrical Engineering, Stanford University, Stanford, California 94305, USA
(Received 16 September 2005; published 24 February 2006)

We show that a metal-dielectric-metal structure can function as a negative refraction lens for surface plasmon waves on a metal surface. The structure is uniform with respect to a plane of incidence and operates at the optical frequency range. Using three-dimensional finite-difference time-domain simulations, we demonstrate the imaging operation of the structure with realistic material parameters including dispersions and losses. Our design should facilitate the demonstration of many novel effects associated with negative refraction on chip at optical wavelength ranges. In addition, this structure provides a new way of controlling the propagation of surface plasmons, which are important for nanoscale manipulation of optical waves.

All-angle negative refraction of electromagnetic waves [1,2] has generated great recent interest because it is the foundation of a variety of new electromagnetic effects and applications, such as subwavelength image formation [2], negative Doppler shift [1], as well as novel guiding, localization and nonlinear phenomena [3,4]. Tremendous progress has been made in achieving negative refraction using either dielectric photonic crystals [5–9] or metallic meta-materials [10–17]. For either approach, however, there is an underlying physical length scale that sets a fundamental limit [18]. Below such a length scale, the concept of an effective index no longer holds. For photonic crystals, it is the periodicity which is smaller than but comparable to the operating wavelength of light [7]. For metallic meta-materials, it is the size of each individual resonant element. In the microwave wavelength range, constructing resonant elements that are far smaller than the operating wavelength is relatively straightforward. As one pushes towards shorter optical wavelength ranges, however, it becomes progressively more difficult to construct resonant elements that are at a deep subwavelength scale [16]. Moreover, in the optical wavelength range, the plasmonic effects of metals become prominent. The strong magnetic response of metallic structures, as observed in microwave and infrared wavelength ranges, may be fundamentally affected. From this perspective, it is very desirable to accomplish all-angle negative refraction using structures that are flat at an atomic scale. Along this direction, a flat metal lens has been experimentally demonstrated using surface plasmons [19]. However, the structure does not operate on the propagating components of a source [2]. Also, achieving a negative refractive index using non-magnetic media has been suggested [20,21]. However, it is not clear yet what uniform physical medium would possess the required dielectric dispersion properties.

Here we introduce a negative refraction lens for propagating surface plasmon waves [Fig. 1(a)]. The lens, consisting of a metal-dielectric-metal (MDM) structure, is uniform with respect to a plane of incidence and is capable of focusing propagating surface plasmon waves on the metal surface at all incidence angles. We demonstrate its operation using the three-dimensional finite-difference time-domain (FDTD) method [22,23]. Our simulations also show that the lens can function even in the presence of losses that are inevitable in realistic materials.

To highlight the essential physics in this structure, we begin by describing the dielectric function of the metal with a lossless free-electron Drude model:

$$\varepsilon(\omega) = 1 - \frac{\omega_p^2}{\omega^2}, \tag{1}$$

where ω_p is the bulk plasma frequency of the metal. We also assume both the metals and the dielectric are nonmagnetic (i.e., $\mu = 1$). All the modes in Fig. 1 have TM polarization with the magnetic field perpendicular to the wave propagation direction. For a single metal-air interface, surface plasmons exist in the frequency range below the frequency $\omega_{\text{sp air}} = \omega_p/\sqrt{2}$, and the band has a positive slope at all frequencies [Fig. 1(b), left panel]. In contrast, for the MDM structure, there are three bands of modes whose fields are guided in the dielectric region [Fig. 1(b), right panel] [24]. At $k_z \rightarrow \infty$, the first two bands approach $\omega_{\text{sp diel}} = \frac{\omega_p}{\sqrt{1+\varepsilon_d}}$. (Here, ε_d is the dielectric constant of the dielectric region.) For the second band, at $k_z = 0$, its frequency $\omega_{\text{II}}(k_z)$ depends on the dielectric thickness d. When $d < \frac{\lambda_p}{4} \frac{\sqrt{1+\varepsilon_d}}{\sqrt{\varepsilon_d}}$ where $\lambda_p = \frac{2\pi c}{\omega_p}$ and c is the velocity of light in vacuum, $\omega_{\text{II}}(k_z = 0)$ becomes greater than $\omega_{\text{sp diel}}$ and the band acquires a negative slope and a negative group velocity [25].

For the MDM structure, the negative group velocity is related to the negative power flow of the mode. For any given eigenmode, the time-averaged Poynting vector always changes sign across a metal-dielectric interface, since the displacement fields normal to the interface are continu-
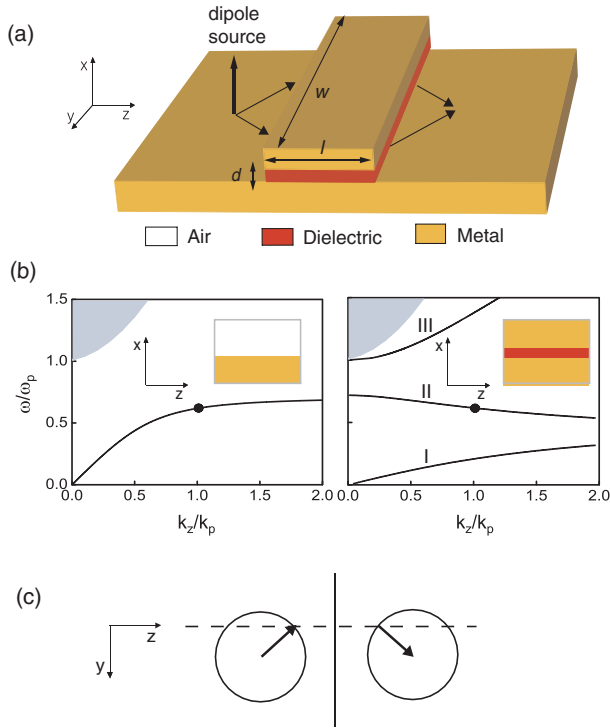
FIG. 1 (color). (a) The geometry of an imaging system consisting of a stripe of a MDM structure on a metal surface. The arrows on the metal surface indicate the lens operation. (b) The dispersion relations for modes of a metal-air interface (left panel), and for modes in an MDM structure with $d = 0.1\lambda_p$ and $\varepsilon_d = 4$ (right panel). The corresponding structures are shown in the inset. The gray areas represent the continuum of extended modes in metal regions. ω_p is the bulk plasma frequency of the metal, and $k_p \equiv \omega_p/c$, respectively. The black dots in both figures indicate the frequency ω_0 at which the wave vectors of the modes in the two structures match in magnitude. (c) The constant frequency contours at ω_0 for both the metal-surface region (left side) and the MDM region (right side). The solid line in the middle represents the boundary of the two regions. The arrows indicate the group velocity directions. The dashed line represents the condition for conservation of wave vectors parallel to the boundary.

ous, and the dielectric constant of the metal region is negative. As a result, the Poynting vector inside the metal is opposite to the phase velocity. For the MDM structure, the modes in the second band can have more power in metal than in dielectric, resulting in the net power flow that is opposite to the phase velocity [26].

The second band for the MDM structure and the surface plasmon for the metal-air interface overlap in frequency when $\varepsilon_d > 1$. With a proper choice of the dielectric thickness, the MDM region can therefore function as a negative refraction lens for the propagating surface plasmon waves on the metal-air interface (Fig. 1). Since the MDM structure by itself is uniform in all directions parallel to the metal surface, the constant frequency contour is *exactly* circular at all frequencies, which distinguishes it against all

previously demonstrated physical realization of negative index media. In addition, one can choose an operating frequency such that the wave vectors in the two regions become equal in length, and thus the effective phase index of the two regions are matched in magnitude [Fig. 1(c)]. The phase-index matching ensures negative refraction at all angles of incidence, as well as aberration-free image formation, as one can show using Fourier decomposition.

In our design, there are reflections at the boundaries between regions due to modal mismatch. This can be seen by analyzing the modal profile for the two structures shown in Fig. 1(b) at the index matching frequency. On the metal-air interface, the mode intensity has a single maximum at the interface [Fig. 2(a), left panel], while the mode intensity in the MDM region has two maxima on the two metal-dielectric interfaces [Fig. 2(a), right panel]. To optimize modal overlap, instead of using the "homo-MDM" structure, where both the top and the bottom metals are of the same kind, one can use a "hetero-MDM" structure, where the metals have different bulk plasma frequencies, to
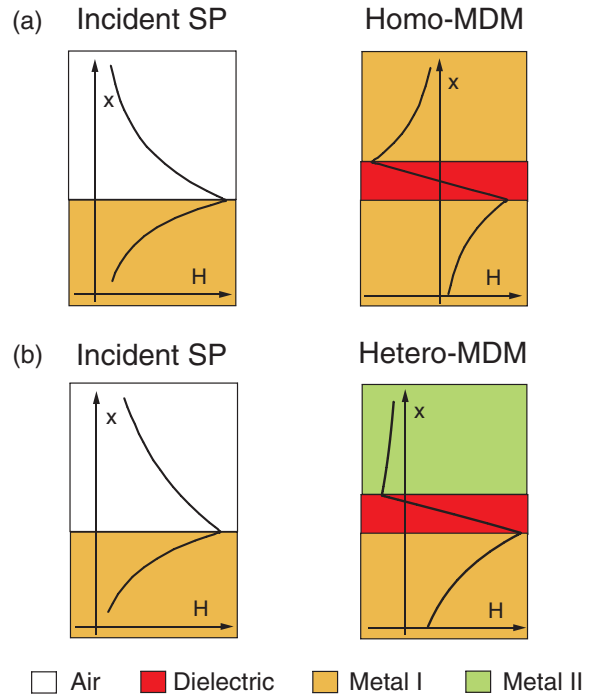

FIG. 2 (color). The magnetic field profiles for: (a) A mode of the metal-air interface (left panel) and a mode in the second band of a homo-MDM structure (right panel). All metals have the same plasma frequency ω_p; the dielectric region has a thickness of $0.1\lambda_p$ and a dielectric constant of 4. Both modes have the same frequency $0.62\omega_p$ and the same wave number k_p. (b) A mode of the metal-air interface (left panel) and a mode in the second band of a hetero-MDM structure (right panel). The metal at the top has a plasma frequency $\omega_p' = 0.6\omega_p$. The dielectric region has the thickness of $0.1\lambda_p$ and the dielectric constant of 4. Both modes have the same frequency $0.539\omega_p$ and the same wave number $0.69k_p$.

break the symmetry of the field profile and enhance the fractional amplitude of the peak at the lower interface [Fig. 2(b)].

We now demonstrate the lens operation of a hetero-MDM structure. We choose $\omega'_p = 0.6\omega_p$, where ω_p and ω'_p are the bulk plasma frequencies of the lower and upper metal sections, respectively [27]. The MDM region has $d = 0.1\lambda_p$, $w = 8.67\lambda_p$, and $l = 2.5\lambda_p$ where w and l are the width and the length of the MDM, respectively [See Fig. 1(a)]. The dielectric region has $\varepsilon_d = 4$. The simulations use FDTD method in three dimensions with a grid size of $\lambda_p/120$. The material dispersion is treated using an auxiliary differential equation method [22]. The computational cell is surrounded by the perfectly matched layer absorbing boundary condition [28]. We assume a near-lossless Drude model for the metals with the collision frequencies set at one-thousandth the bulk plasma frequencies. We excite surface plasmon waves on the left region of the metal surface by placing a single dipole source at λ_p away from the edge of the MDM. The source has a frequency of $\omega = 0.539\omega_p$ and is polarized perpendicular to the metal surface. The steady-state field distribution for the x component of the electric field is shown in Fig. 3(a). Two images are observed: one near the center in the MDM region, and the other on the right region of the metal surface. Also, we observe significant field enhancement at the boundaries of the MDM, indicating excitation of edge states [29]. [The actual field values at the boundaries are underrepresented in Fig. 3(a), due to the color scheme chosen which saturates at large field values in order to highlight the image.]

Our calculations show that such a lens can resolve two sources, oscillating in phase, with a distance of $0.93\lambda_p$ between them [Fig. 3(b)]. In comparison, at this operating frequency $\omega = 0.539\omega_p$, the surface plasmon wave at the metal-air interface has a wavelength of $1.46\lambda_p$. We do not observe perfect image recovery. This is consistent with previous FDTD simulations on ideal negative index lens with ε and μ simultaneously negative [29–31]. In addition to computational constraints due to finite widths [29] and numerical dispersions for large wave vector components [30], Smith *et al.* have shown theoretically that for a lens with length comparable to the wavelength of incident wave, to achieve perfect imaging requires parameter accuracy that is very difficult to realize in either simulations or experiments [18].

For practical plasmonic structures, material loss is a major issue. The effect of losses in metal can potentially be mitigated by operating at low temperature [32], or by introducing gain [33]. For our structure, even in the presence of the realistic material loss, the lens can still function with proper design. As a demonstration, we use as the MDM lens a Ag-GaP-Ag structure with a length of 280 nm, a width of 1440 nm and a dielectric thickness of 24 nm. The surface of Ag outside the MDM region is
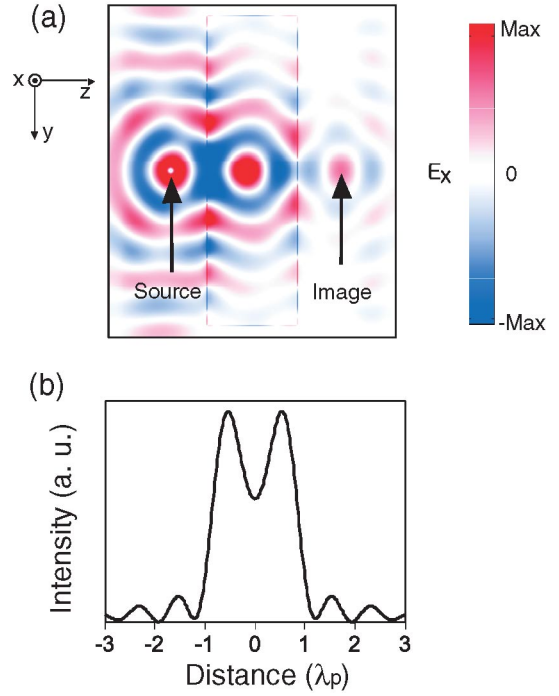

FIG. 3 (color). The imaging process for surface plasmons with a hetero-MDM lens. The computational set up is schematically shown in Fig. 1. (a) Plotted here is the steady-state E_x field distribution on a cross section at $0.18\lambda_p$ above the bottom metal surface. The color scheme is chosen to saturate at large field values in order to show the formed image clearly. (b) The time average E_x field intensity at the image plane for two point sources oscillating in phase. The lens has a length of $1.7\lambda_p$. The two point sources are separated by $0.93\lambda_p$ apart, and are placed at $0.5\lambda_p$ away from the edge of the lens. In comparison, at the operating frequency $\omega = 0.539\omega_p$, the surface plasmon wave at the metal-air interface has a wavelength of $1.46\lambda_p$.

covered by a 28 nm thick Si_3N_4 film with a refractive index of 2 [Fig. 4(a)]. The use of GaP and Si_3N_4 pushes the operating free-space wavelength up to 479 nm where Ag has less loss. At this wavelength, there is absorption loss from GaP. However, the overall loss of the structure is still lower compared with structures operating at shorter wavelengths, since the loss in Ag increases dramatically as wavelength decreases. To simulate this structure with FDTD, we fit the experimentally determined dielectric constants [34] of Ag and GaP with Lorentz-Drude models. At the operating wavelength, our models give $\varepsilon_{Ag} = -7.47 - i0.73$ and $\varepsilon_{GaP} = -13.69 - i0.045$, which agrees excellently with experimental values for these materials [34]. The grid size is chosen to be 2 nm. The dipole source is placed on the Ag surface 40 nm away from the edge of the MDM region. Figure 4(b) shows the E_x field profile at steady state. Although the amplitude of the transmitted wave is strongly attenuated due to reflection and material losses, the image formation is still clearly visible.
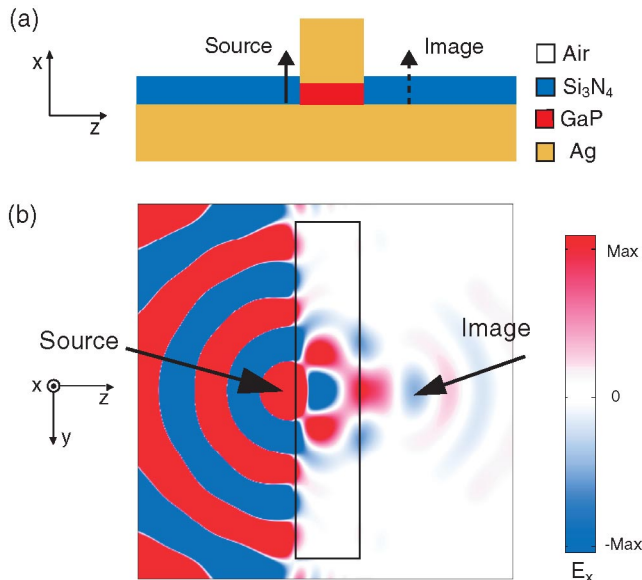
FIG. 4 (color). (a) Cross-sectional view of a simulated structure for the purpose of demonstrating imaging process with realistic material parameters. The solid and dashed arrows indicate the positions of the source and the image, respectively. (b) Steady-state E_x field for the structure shown in Fig. 4(a), on a cross section at 60 nm above the bottom Ag surface.

We have identified a new route towards all-angle negative refraction. The simplicity of the MDM structures should enable one to incorporate negative index materials into geometries that are more complex than a flat lens, which can lead to a wide range of unexplored novel electromagnetic effects [35]. The proposed structure also provides a new mechanism for controlling the propagations of surface plasmons, which are important for manipulating light at nanoscale [36]. In conclusion, we believe this work could facilitate the eventual demonstration of many important effects associated with negative refraction on chip in the optical wavelength ranges.

[1] V. G. Veselago, Sov. Phys. Usp. **10**, 509 (1968).
[2] J. B. Pendry, Phys. Rev. Lett. **85**, 3966 (2000).
[3] I. V. Shadrivov, A. A. Sukhorukov, and Y. S. Kivshar, Phys. Rev. Lett. **95**, 193903 (2005).
[4] G. D'Aguanno, N. Mattiucci, M. Scalora, and M. J. Bloemer, Phys. Rev. Lett. **93**, 213902 (2004).
[5] M. Notomi, Phys. Rev. B **62**, 10 696 (2000).
[6] C. Luo, S. G. Johnson, J. D. Joannopoulos, and J. B. Pendry, Phys. Rev. B **65**, 201104 (2002).
[7] C. Luo, S. G. Johnson, J. D. Joannopoulos, and J. B. Pendry, Phys. Rev. B **68**, 045115 (2003).
[8] E. Cubukcu, K. Aydin, E. Ozbay, S. Foteinopolou, and C. M. Soukoulis, Phys. Rev. Lett. **91**, 207401 (2003).
[9] A. Berrier, M. Mulot, M. Swillo, M. Qiu, L. Thylen, A. Talneau, and S. Anand, Phys. Rev. Lett. **93**, 073902 (2004).
[10] J. B. Pendry, A. J. Holden, W. J. Stewart, and I. Youngs, Phys. Rev. Lett. **76**, 4773 (1996).
[11] J. B. Pendry, A. J. Holden, D. J. Robbins, and W. J. Stewart, IEEE Trans. Microwave Theory Tech. **47**, 2075 (1999).
[12] D. R. Smith, W. J. Padilla, D. C. Vier, S. C. Nemat-Nasser, and S. Schultz, Phys. Rev. Lett. **84**, 4184 (2000).
[13] R. A. Shelby, D. R. Smith, and S. Schultz, Science **292**, 77 (2001).
[14] T. Koschny, M. Kafesaki, E. N. Economou, and C. M. Soukoulis, Phys. Rev. Lett. **93**, 107402 (2004).
[15] T. J. Yen, W. J. Padilla, N. Fang, D. C. Vier, D. R. Smith, J. B. Pendry, D. N. Basov, and X. Zhang, Science **303**, 1494 (2004).
[16] S. Linden, C. Enrich, M. Wegener, J. Zhou, T. Koschny, and C. M. Soukoulis, Science **306**, 1351 (2004).
[17] J. B. Pendry, Science **306**, 1353 (2004).
[18] D. R. Smith, D. Schurig, M. Rosenbluth, S. Schultz, S. A. Ramakrishna, and J. B. Pendry, Appl. Phys. Lett. **82**, 1506 (2003).
[19] N. Fang, H. Lee, C. Sun, and X. Zhang, Science **308**, 534 (2005).
[20] Y.-F. Chen, P. Fischer, and F. W. Wise, Phys. Rev. Lett. **95**, 067402 (2005).
[21] V. A. Podolskiy and E. E. Narimanov, Phys. Rev. B **71**, 201101 (2005).
[22] A. Taflove and S. C. Hagness, *Computational Electrodynamics: The Finite-Difference Time-Domain Method* (Artech House, Norwood, 2005).
[23] K. S. Yee, IEEE Trans. Antennas Propag. **14**, 302 (1966).
[24] E. N. Economou, Phys. Rev. **182**, 539 (1969).
[25] H. Shin, M. F. Yanik, S. Fan, R. Zia, and M. L. Brongersma, Appl. Phys. Lett. **84**, 4421 (2004).
[26] P. Tournois and V. Laude, Opt. Commun. **137**, 41 (1997).
[27] The ratio used here corresponds to the ratio between the plasma frequencies of Al (14.98 eV) and Ag (9.01 eV) in typical Drude models. See A. D. Rakic *et al.*, Appl. Opt. **37**, 5271 (1998).
[28] J. P. Berenger, J. Comput. Phys. **114**, 185 (1994).
[29] L. Chen, S. He, and L. Shen, Phys. Rev. Lett. **92**, 107404 (2004).
[30] S. A. Cummer, Appl. Phys. Lett. **82**, 1503 (2003).
[31] R. W. Ziolkowski and E. Heyman, Phys. Rev. E **64**, 056625 (2001).
[32] A. Karalis, E. Lidorikis, M. Ibanescu, J. D. Joannopoulos, and M. Soljacic, Phys. Rev. Lett. **95**, 063901 (2005).
[33] S. A. Ramakrishna and J. B. Pendry, Phys. Rev. B **67**, 201101 (2003).
[34] E. D. Palik, *Handbook of Optical Constants of Solids* (Academic Press, San Diego, 1985).
[35] J. B. Pendry and S. A. Ramakrishna, J. Phys. Condens. Matter **14**, 8463 (2002).
[36] W. L. Barnes, A. Dereux, and T. W. Ebbesen, Nature (London) **424**, 824 (2003).